Vol. 603: 265–272, 2018
https://doi.org/10.3354/meps12727

MARINE ECOLOGY PROGRESS SERIES
Mar Ecol Prog Ser

Published September 17

NOTE

Ecological consequences of internal seiches in a semi-enclosed, anoxic coastal basin

S. Kelly[1, 2,*], E. de Eyto[2], R. Poole[2], M. White[1]

[1]Earth & Ocean Science, National University of Ireland Galway, Galway, H91 TK33, Ireland
[2]Marine Institute, Newport, Mayo, F28 PF65, Ireland

ABSTRACT: Climate-related increase of near-surface water temperatures in aquatic environments both decreases oxygen solubility and intensifies vertical stratification of the water column, prompting concern over the depletion of dissolved oxygen (DO) in deep interior waters. Understanding bio-physical interactions in affected ecosystems is therefore paramount, as physical processes often determine the spatial extent of deoxygenated zones. One pertinent example, often linked to mass-mortality events of marine organisms, is wind-driven upwelling of low-DO deep waters into shallower, nearshore oxygenated areas. In this note, mortalities recorded during routine fishery surveys in Lough Furnace, a semi-enclosed estuarine basin with deep anoxia, are shown to result from significant wind events. Advection of deoxygenated deep water into nearshore areas occupied by fishing nets occurred following strong winds. Relaxation of the initial wind stress generated a baroclinic standing wave (internal seiche) and a succession of upwelling and downwelling events which caused drastic fluctuations in nearshore DO concentrations that persisted for several hours. The internal seiche dynamics were confirmed following analysis of water density oscillations at a mid-basin and boundary location. These results highlight the importance of bio-physical interactions in aquatic ecosystems with DO-depleted deep waters, as hydrodynamic processes can mediate the exposure of biota to deoxygenated water conditions.

KEY WORDS: Anoxia · Fish kill · Upwelling · Stratification · *Anguilla anguilla*

INTRODUCTION

Dissolved oxygen (DO) depletion in aquatic environments is a growing concern globally, with profound negative implications for biodiversity and ecosystem productivity (Diaz & Rosenberg 2008, Breitburg et al. 2018). Climate change is anticipated to intensify deoxygenation in bottom waters, with warming of near-surface waters decreasing oxygen solubility and strengthening stratification of the water column, limiting downward mixing of DO-rich surface water (Keeling et al. 2010). This climate-related escalation of bottom water DO depletion is expected to affect oceans (Schmidtko et al. 2017), coastal and estuarine systems (Zhang et al. 2010) and freshwater lakes (North et al. 2014). Microbial degradation of organic material in the water column and bottom sediments consumes DO, and in isolated bottom waters without a replenishing DO source, hypoxic (<2 mg O_2 l^{-1}) and eventually anoxic (0 mg O_2 l^{-1}) conditions will develop (Diaz & Rosenberg 2008).

The effects of hypoxia on aerobically respiring aquatic organisms vary from reducing scope for growth and fecundity (Gray et al. 2002) to more insidious effects such as compressing viable habitat

*Corresponding author: Sean.Kelly@marine.ie

space and necessitating changes in movement and feeding behaviours (e.g. Wannamaker & Rice 2000, Domenici et al. 2007). Hydrogen sulphide (H_2S) is a microbial by-product of anoxic conditions and toxic to aerobic species (Vacquer-Sunyer & Duarte 2010), giving anoxic H_2S-rich water the capacity to cause mass mortalities of aquatic organisms during single exposure events (e.g. Luther et al. 2004).

In stratified waters with deep hypoxic/anoxic zones isolated from oxygenated upper layers by a stable density gradient (pycnocline), an important consideration is the effect of wind-induced upwelling events, where an episodic upslope movement of deoxygenated sub-pycnocline water masses into shallower nearshore oxygenated refuges occurs. This phenomenon has been previously documented in coastal ecosystems (e.g. Grantham et al. 2004), estuaries (e.g. Sanford et al. 1990, Reynolds-Fleming & Luettich 2004), saline lagoons (e.g. Chikita 2000) and lakes (e.g. Bernhardt et al. 2014). In confined basins, wind-driven surface currents are piled against the downwind basin boundary, raising the surface water level at this end. This horizontal pressure gradient leads to a depression in the pycnocline below its equilibrium depth (downwelling) at the downwind end. This is balanced by a return flow of deeper water and an uptilt of the pycnocline at the upwind boundary (upwelling) (e.g. Shintani et al. 2010). Calming of the initial wind stress allows the tilted condition of the pycnocline to relax back toward its equilibrium position with the momentum generating a standing gravitational wave at the pycnocline (internal seiche) which reflects back and forth from each basin end and causes a series of regular, basin-wide internal oscillations (Münnich et al. 1992, Shintani et al. 2010).

In this note, mortalities of European eel *Anguilla anguilla* observed in catches from routine fishery surveys in a stratified estuarine basin with deep anoxia are linked to wind-induced internal seiching and consequent upwelling of anoxic water into susceptible nearshore regions, for which few observations exist. The initial focus was on the gravest internal seiche mode (referred to hereafter as T_1), which shifts the whole water column up and down and has opposite horizontal flow between a surface and bottom layer separated by a pycnocline of constant thickness (e.g. Münnich et al. 1992). Whilst the fishery surveys offered an unusual, opportunistic experiment to test this, the wider ecological implications of upwelling of DO-depleted deep water are considered, as similar physical dynamics related to wind-driven water movements are ubiquitous in stratified water bodies.

MATERIALS AND METHODS

Study site

The study was conducted in Lough Furnace, a semi-enclosed estuarine basin on the Atlantic coast of Ireland (53° 55′ 04″ N, 9° 34′ 20″ W) (Fig. 1). The northern main inner basin (max depth 20 m) receives surface freshwater input from river runoff and tidal inflow of saline water from the southern entrance channel. Tides are semi-diurnal, with spring and neap tidal ranges of 0.3 m and 0.1 m respectively. Stagnant hypoxic and anoxic conditions are typically maintained below 7–8 m (35–40% of the total basin volume) by the strong halocline (usually at 1–4 m depth) and the restricted estuary–ocean exchange, with significant ventilation of the deep water by dense tidal intrusions only occurring at approximately 2-year intervals (Kelly et al. 2018).

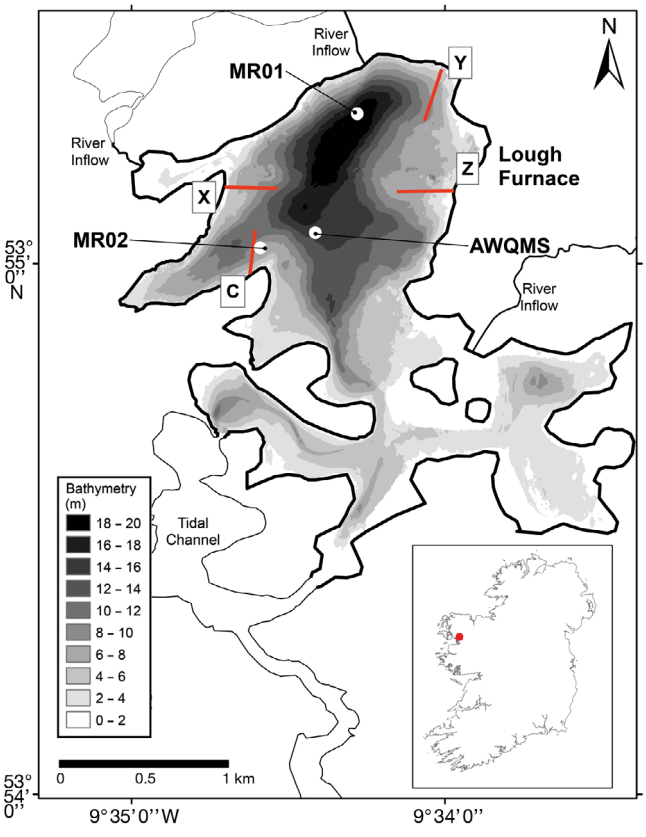

Fig. 1. Lough Furnace (thick outline is the semi-enclosed main basin and thin outline the shallow tidal channel connecting to the ocean) showing fyke net (red lines) and measuring sites: automatic water quality monitoring station (AWQMS); MR01; and MR02 (see Table 1 for mooring instrumentation)

Fishery surveys

Stock assessment surveys for critically endangered European eel *Anguilla anguilla* have been carried out intermittently in Lough Furnace since 1987 and annually since 2011. In these surveys, 10 fyke nets (each 15 m long unit consists of 2 funnel-shaped nets connected by a leading net, with the openings facing each other) are joined together end-to-end to form a single net chain laid along the bed starting at the shoreline and extending ~150 m directly offshore (Poole & Reynolds 1996). Fyke net locations are shown in Fig.1, with dead eels often recovered at site C (see Table 2). Given the frequency of westerly winds in this system (Kelly et al. 2018), it was hypothesised that the location of site C near the shallower western side of the main basin would make it susceptible to upwelling of deep anoxic water. This was tested during two 2016 fyke net surveys, S1 and S2 (Table 1). Numbers of live and dead eels per net were recorded, and dead eels were sampled for signs of injury and for stomach contents.

Hydrographic observations

Table 1 summarises instruments deployed during each net survey, and Fig. 1 indicates locations of moorings MR01 and MR02. In addition to these moorings, transects of DO depth profiles measured at 0.15 m increments were made using a handheld probe (*In-Situ* smarTROLL) at 4 locations along the length of each fyke net chain, immediately after nets had been set (Table 1). An echosounder transect from 165 m offshore to the shoreline was taken to assess bathymetry at net sites. Wind speed and direction at 2 min intervals and water column profiles of density and DO every 6 h (using a Hydrolab DS5 data sonde attached to an undulating winch) were recorded from an automatic water quality monitoring station (AWQMS) in the central basin (Fig. 1). Both S1 and S2 occurred during neap tidal phases (<0.1 m change in water level height).

The internal wave field was assessed using normal mode analysis of the density stratification. Density profiles measured at the AWQMS (at 0.15 m increments) were averaged for the duration of S1 and S2 and used to calculate vertical profiles of the buoyancy frequency squared: $N^2(z) = (-g/\rho)\, d\rho/dz$, where g is gravity, ρ is density and z is depth. By imposing rigid level boundary conditions at the surface ($z = 0$) and bottom ($z = -H$, where H is the full water column depth), and in the absence of background shear, the modal structure and corresponding phase speeds of long, linear internal wave motions that would result from an initial perturbation to a stratified fluid characterised by $N^2(z)$, were determined through solution of the eigenvalue problem (e.g. Gill 1982):

$$\frac{d^2\psi_i(z)}{dz^2} + \frac{N^2(z)}{c_i^2}\psi_i(z) = 0 \quad (1)$$

$$\psi(-H) = \psi(0) = 0 \quad (2)$$

where the eigenfunction $\psi_i(z)$ and its eigenvalue c_i are the vertical modal structure and phase speed respectively of a horizontally propagating wave of the i^{th} vertical mode. The largest eigenvalue is the phase speed of the fundamental baroclinic mode (c_1) and was used to estimate T_1 for S1 and S2, with $T_1 = 2L/c_1$, where L is an effective horizontal scale (i.e. basin length at the pycnocline depth along the axis of wind forcing).

Time series of water densities were calculated for each sensor at moorings MR01 and MR02 for the 5 d period overlapping with the S2 survey (Table 1). Spectral analysis was carried out on each time series by calculating power spectra and 95% confidence intervals using a multitaper spectrum estimate (Rahim & Burr 2014) in R version 3.3.3 (R Core Team 2017). Water density at 3 m at MR01 and MR02 was analysed to compare vertical oscillations between the site C net location and at a location near the opposite side of the basin.

Table 1. Schedule of fishery surveys S1 and S2 with measurement details taken during each survey. See Fig. 1 for location details

Survey/measurement	Location	Depth (m)	Sampling interval (min)	Date	Time UTC (h)
S1	C, X, Y, Z			13–14 June	~15:00–10:00
DO transect	C			13 June	~15:30–16:15
DO sensor (JFE Advantech ARO-USB)	MR02	7.5	5	13–14 June	15:00–15:00
S2	C, X, Y, Z			28–29 June	~15:00–10:00
DO transect	C			28 June	~15:30–16:15
Temperature/salinity (Sea-Bird Scientific SBE-37)	MR01	1, 3, 5, 7	5	27–02 July	15:00–14:00
Temperature/salinity (Sea-Bird Scientific SBE-37)	MR02	3, 7	5	27–02 July	15:00–14:00

RESULTS

Fishery surveys

Anoxic water spatially overlapped with the outermost parts of the site C net chain during both surveys (Fig. 2). Eleven eels were captured during survey S1 at site C (Table 2) with dead eels recovered in the outermost nets containing any catch (10 and 8) and the remaining live catch in nets 1, 2 and 5. One dead eel was recovered from site Y (net 10) with no mortalities in sites X or Z. For survey S2, dead eels were recovered from site C in nets 4 and 6, at depths that initially did not experience severely low-DO conditions (Fig. 2c); interestingly, live eels were also recovered in deeper nets 6 and 5 (in addition to 4 eels in net 1) (Table 2). Dead eels were also discovered at site X (net 8) and site Y (net 10).

Dead eels showed no evidence of clogged gill tissue or obvious disease or injury. Eight of 9 fish had full stomachs, indicative of recent feeding. Several dead fish had wide, open mouths and expanded gills upon initial recovery, likely a symptom of having been asphyxiated.

Hydrography

During survey S1, winds were primarily northerly, occasionally veering westerly (Fig. 3a). Comparison of bottom DO concentrations with the wind stress indicates that a downwelling of oxygenated surface water occurred initially as the northerly wind blew surface water toward site C (between 15:00 and 19:00 h; Fig. 3a,b). Relaxation of the wind generated a baroclinic seiche, evident as 5 successive upwelling and downwelling events in the MR02 DO time series during the ensuing calmer period (from 19:30 to 07:00 h; Fig. 3b). A periodogram of the DO time series during this post-wind focal period revealed a prominent periodicity of 2 h (Fig. 3c). Another strong wind from the north at ~07:00 h disturbed this internal seiche by causing another downwelling event and possibly re-energising a second internal seiche (up-

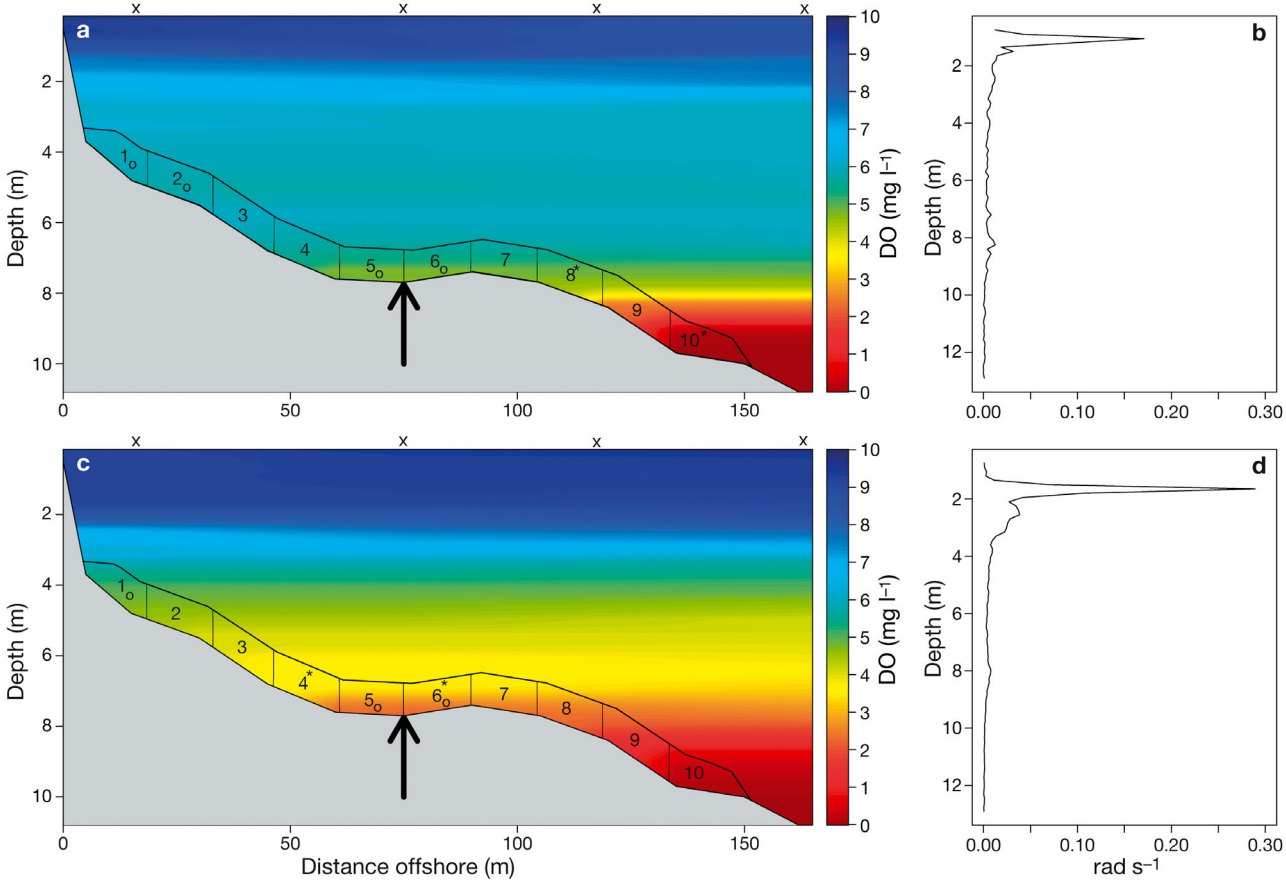

Fig. 2. (a) Dissolved oxygen (DO) transect at site C ('x' indicates profile locations); (b) average buoyancy frequency squared (N^2) profile for S1; (c) and (d) show the same for S2. Schematic illustration of fyke net chain in (a) and (c) with nets 1–10 numbered (recovery of live eels denoted by the subscript 'o', of dead eels by superscript '*'). Arrows indicate location of MR02

Table 2. Total eel catch per net during surveys S1 and S2 and total historical catch at site C. Number of dead eels per net indicated in parentheses. Net 1 is inshore and net 10 furthest offshore (see Fig. 2)

Survey	Site	Net									
		10	9	8	7	6	5	4	3	2	1
S1	C	2 (2)	0	1 (1)	0	1	3	0	0	2	2
	X	0	0	2	1	2	1	0	0	0	0
	Y	2 (1)	0	2	2	1	0	0	2	3	2
	Z	5	0	5	1	1	2	0	5	1	0
S2	C	0	0	0	0	2 (1)	1	1 (1)	0	0	4
	X	0	0	2 (2)	0	0	1	2	2	1	1
	Y	1 (1)	0	0	1	1	1	2	2	5	1
	Z	0	0	0	0	1	1	3	1	4	0
Historic	C	12 (6)	31 (12)	32 (9)	19 (4)	31 (6)	32 (8)	40 (8)	28 (2)	23 (2)	36

welling of low DO water at ~11:00 h). T_1 calculated for the ~1100 m NW–SE basin axis (roughly aligned with the predominant wind direction during S1) was 2.03 h (c_1 = 0.30 m s^{-1}, using the N^2 profile in Fig. 2b), confirming that the DO oscillations matched the fundamental internal seiche period (Fig. 3c).

The timeseries of wind during the S2 survey and overlapping observation period showed that winds were predominantly westerly with southerly and northerly components (Fig. 4a). Contrasting the initial downwelling during S1, strong westerly winds at the onset of S2 caused upwelling of low-DO water into shallower regions (Figs. 2c & 4a). Water density fluctuations from the daily mean value at 3 m at MR01 and MR02 showed distinct oscillations, with values periodically increasing and decreasing above and below the mean; fluctuations also appeared directly out of phase

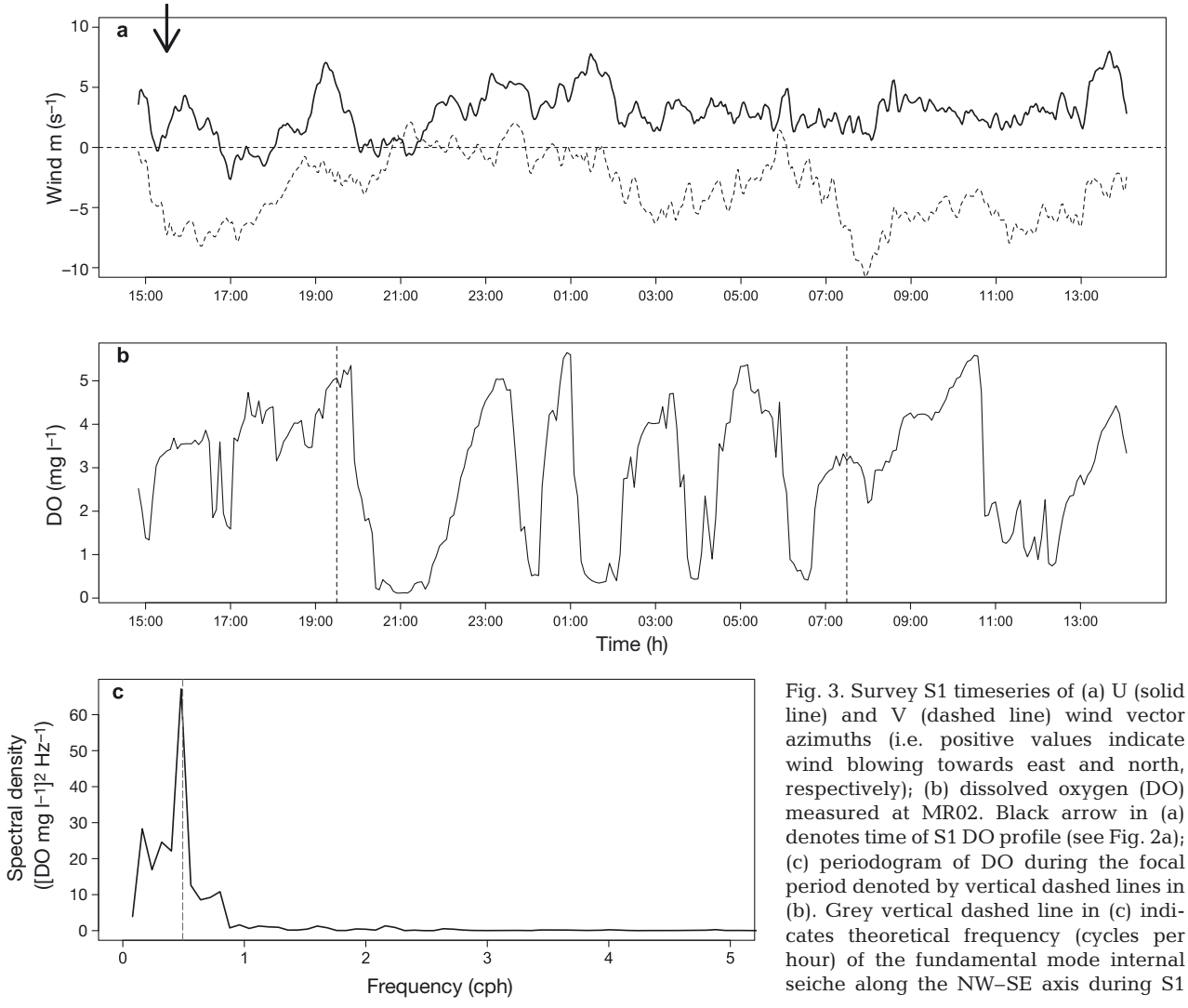

Fig. 3. Survey S1 timeseries of (a) U (solid line) and V (dashed line) wind vector azimuths (i.e. positive values indicate wind blowing towards east and north, respectively); (b) dissolved oxygen (DO) measured at MR02. Black arrow in (a) denotes time of S1 DO profile (see Fig. 2a); (c) periodogram of DO during the focal period denoted by vertical dashed lines in (b). Grey vertical dashed line in (c) indicates theoretical frequency (cycles per hour) of the fundamental mode internal seiche along the NW–SE axis during S1

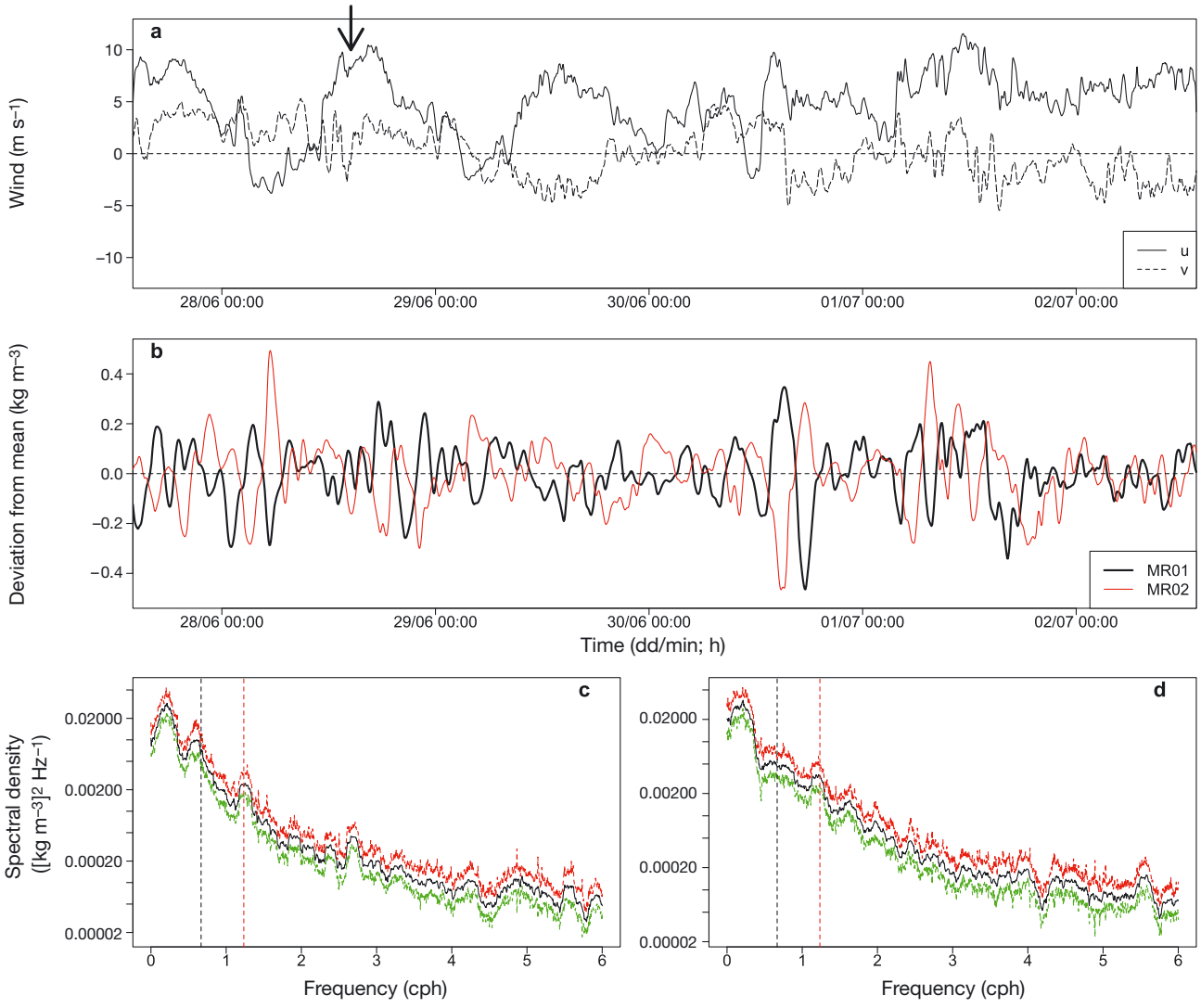

Fig. 4. Survey S2 timeseries of (a) U (solid line) and V (dashed line) wind vector azimuths (i.e. positive values indicate wind blowing towards east and north, respectively) and (b) comparison of water density deviations from the daily mean value at 3 m depth at MR01 and MR02. Black arrow in (a) denotes time of S2 dissolved oxygen profile (Fig. 2c); (c) spectral density (black line) and 95% confidence intervals (red and green dashed lines) for the S2 water density timeseries at 3 m for MR01; (d) shows the same for MR02. Vertical dashed lines in (c) and (d) show fundamental mode internal seiche frequencies (cycles per hour) along the SW–NE axis (black) and E–W axis (red) of the main basin during S2

between the 2 locations (Fig. 4c). Spectral analysis of the water density at 3 m for MR01 (Fig. 4c) and MR02 (Fig. 4d) showed pronounced spectral peaks at ~1.25 cycles per hour (cph) with MR01 also showing a peak at ~0.6 cph (although a flatter peak around this frequency was also observable for MR02).

Between S1 and S2, the upper freshwater layer deepened following rainfall events and stratification was greater during S2, resulting in a higher c_1 value calculated from the mean N^2 profile for this period (Fig. 2d) of 0.44 m s^{-1}. Using this phase speed and considering the main wind dynamics, T_1 was calculated for a wave travelling directly across the E–W axis of the main basin (~650 m) and also across the longer NE–SW axis (~1200 m, slightly longer than the NW–SE axis). T_1 across the shorter E–W axis was 0.81 h and along the longer NE–SW axis was 1.5 h. Both T_1 values appeared to correspond with peaks in the MR01 and MR02 power spectra, which were more apparent for the MR01 site, possibly related to larger internal wave amplitudes in this deeper part of the basin (Fig. 4c,d)

A spectral peak was also observable at the lower frequency of ~0.25 cph (~4 h periodicity) for both MR01 and MR02 (Fig. 4c,d). Given the estimated phase speeds of the first few vertical wave modes

and basin geometry, it appears that this peak was not directly related to a cross-basin, wind-generated internal seiche with a central nodal point. It is proposed that the origin of this 4 h periodicity may therefore be related to a tidally-forced pycnocline displacement originating from the open mouth at the southern end of the main basin (Fig. 1). This open boundary represents a nodal line, since external water masses outside the inner basin are involved in the seiche oscillations, and therefore the gravest mode response to tidal forcing occurring through the (narrow) entrance channel is a progressive standing wave radiating away from the node with a wavelength of 4 times the basin length (e.g. Wilson 1972). By using the range of c_1 values calculated (0.3 to 0.44 m s^{-1}) and a basin length from the mouth to the northern boundary of ~1200 m, a resulting seiche period of 3 to 4.4 h was estimated, which may explain these lower frequency density oscillations at 3 m for MR01 and MR02, noted in Fig. 4c,d.

In the immediate aftermath of each pronounced wind event (wind >8–10 m s^{-1}) density oscillations at 3 m appeared directly out of phase between MR01 and MR02 (Fig. 4b). Vertical displacement of water masses in different directions at opposite basin ends along the general axis of wind stress (E–W or NE–SW) led to the conclusion that the initial major fluctuations observed in DO (S1) and density (S2) appeared to be correlated to the mode 1 internal seiche response to cross-basin wind-forcing (Figs. 3 & 4). Subsequent density oscillations were generally not directly out of phase between MR01 and MR02, often appearing to be of similar phase. This was consistent with a seiche, likely tidally-forced, propagating south–north (i.e. from the mouth to the head), with MR01 and MR02 both located north of the entrance channel. The significance of this lower frequency (~0.25 cph) oscillation for nearshore DO remains unclear.

DISCUSSION

Results indicated that dissolved oxygen fluctuations, related to wind-induced baroclinic motions, led to mortalities in captured fish held in nearshore areas that are within the upwelling limits of deoxygenated water from the deep zone of the main basin.

The fishery surveys offered a novel method for assessing the extent of upwelling and subsequent biophysical interactions. Whilst the setting was unnatural (i.e. captured eels were unable to escape from developing harmful conditions) they illustrated the potential implications of deoxygenated deep water for commercial fisheries in similar habitats, which could experience a reduction in viable catch or fishing grounds. Eels were obviously alive as they entered a specific net location meaning that DO conditions were reasonably favourable at that time and location. Thus, if an eel enters a deeper, offshore net during a downwelling phase it cannot escape and move to a shallower net in the event of a subsequent upwelling, likely explaining why eels were caught in nets which normally experience very low DO concentrations.

Using the slowest baroclinic wave speed (c_1 = 0.30 m s^{-1}), the Rossby radius of deformation (L_R = c_1/f, where f is the latitude-dependent Coriolis frequency) was 2500 m. The ratio of L_R to the radius of the basin's major axis was 4.2, allowing any weak rotational influence to be discounted for the present analysis (e.g. Gill 1982). Spectral analysis of the wind data (not shown) indicated a pronounced 24 h periodicity in wind speed. The strongest winds occurred in the afternoon, diminishing toward night (Fig. 4a), meaning afternoon wind energy may generate overnight internal seiche activity. In each of the focal periods presented, the most dramatic patterns of upwelling and downwelling were observed during night time hours (Figs. 3b & 4b) when many benthic fish, including eels, actively forage. Tidal forcing may also generate pycnocline oscillations and the influence of these motions on nearshore DO dynamics requires further investigation.

Disproportionately higher numbers of eels caught in shallower nets indicate that eels generally avoid the deep, low-DO zones. However live eels were retrieved from fyke nets that also contained dead eels (Fig. 2c; S2 catch, Table 2); these eels may have only entered the net shortly before nets were recovered or were able to tolerate short periods of deoxygenation. Amongst teleosts, European eel have one of the highest tolerances to low DO, with a critical O_2 value (level below which a stable O_2 uptake cannot be maintained) of ~1 mg l^{-1} (Rogers et al. 2016). Other species however may not share the robustness of eel toward low-DO conditions, as evident in the absence of any other live species in the site C fyke net apart from nets 1 and 2 which contained crab, flounder and pollack. Overall it is noted that historically, eel mortalities amongst the site C catch are generally associated with nets further offshore than inshore, with deep offshore sites more likely to be exposed to deoxygenated water conditions during seiche activity (Table 2).

In a broader context, these findings show that wind-induced baroclinic motions in a stratified basin with deoxygenated bottom waters can dramatically

influence DO conditions in oxygenated nearshore areas that are considered productive fish habitat. Similar episodic movements of seemingly stable, low-DO deep water masses by wind-induced seiching have been documented in very similar environments (Sanford et al. 1990, Chikita 2000, Reynolds-Fleming & Luettich 2004). Therefore, when assessing the spatial extent of hypoxic/anoxic 'dead-zones', a potential exposure zone at shallower depths, particularly around the boundaries where the oxycline meets basin slopes, should be considered. Deoxygenated deep waters may not only affect demersal and benthic fauna, but also nearshore communities inhabiting slopes and banks that are within upwelling limits. Fish movement and feeding may be affected by such upwelling events and sessile or slow-moving benthos may be most vulnerable to lateral intrusions of anoxic water transported upslope by internal waves. Further work is required to assess such bio-physical interactions, with high-resolution acoustic tracking of fish in affected areas in conjunction with hydrographical observations being one potentially informative method.

Acknowledgements. This work was funded by the Marine Institute Cullen Fellowship Programme. The authors sincerely thank David Sweeney, the Marine Institute field staff and Bernadette O'Neill for their invaluable support during this study.

LITERATURE CITED

Bernhardt J, Kirillin G, Hupfer M (2014) Periodic convection within littoral lake sediments on the background of seiche-driven oxygen fluctuations. Limnol Oceanogr Fluids Environ 4:17–33

Breitburg D, Levin LA, Oschlies A, Grégoire M and others (2018) Declining oxygen in the global ocean and coastal waters. Science 359:eaam7240

Chikita K (2000) Dynamic behaviours of anoxic saline water in Lake Abashiri, Hokkaido, Japan. Hydrol Processes 14:557–574

Diaz RJ, Rosenberg R (2008) Spreading dead zones and consequences for marine ecosystems. Science 321:926–929

Domenici P, Lefrançois C, Shingles A (2007) Hypoxia and the antipredator behaviours of fishes. Philos Trans R Soc Lond B Biol Sci 362:2105–2121

Gill AG (1982) Atmosphere–ocean dynamics. In: Donn WL (ed) International geophysics series, Vol 30. Academic Press, London

Grantham BA, Chan F, Nielsen KJ, Fox DS and others (2004) Upwelling-driven nearshore hypoxia signals ecosystem and oceanographic changes in the northeast Pacific. Nature 429:749–754

Gray JS, Wu RS, Or YY (2002) Effects of hypoxia and organic enrichment on the coastal marine environment. Mar Ecol Prog Ser 238:249–279

Keeling RF, Körtzinger A, Gruber N (2010) Ocean deoxygenation in a warming world. Ann Rev Mar Sci 2: 199–229

Kelly S, de Eyto E, Dillane M, Poole R, Brett G, White M (2018) Hydrographic maintenance of deep anoxia in a tidally influenced saline lagoon. Mar Freshw Res 69: 432–445

Luther GW, Ma S, Trouwborst R, Glazer B, Blickley M, Scarborough RW, Mensinger MG (2004) The roles of anoxia, H_2S, and storm events in fish kills of dead-end canals of Delaware inland bays. Estuaries 27:551–560

Münnich M, Wüest A, Imboden DM (1992) Observations of the second vertical mode of the internal seiche in an alpine lake. Limnol Oceanogr 37:1705–1719

North RP, North RL, Livingstone DM, Köster O, Kipfer R (2014) Long-term changes in hypoxia and soluble reactive phosphorus in the hypolimnion of a large temperate lake: consequences of a climate regime shift. Glob Chang Biol 20:811–823

Poole WR, Reynolds JD (1996) Age and growth of yellow eel, *Anguilla anguilla* (L.), determined by two different methods. Ecol Freshwat Fish 5:86–95

R Core Team (2017) R: a language and environment for statistical computing. R Foundation for Statistical Computing, Vienna www.R-project.org

Rahim KJ, Burr WS (2014) multitaper: spectral analysis tools using the multitaper method. R package version 0.9-14. https://CRAN.R-project.org/package=multitaper

Reynolds-Fleming JV, Luettich RA Jr (2004) Wind-driven lateral variability in a partially mixed estuary. Estuar Coast Shelf Sci 60:395–407

Rogers NJ, Urbina MA, Reardon EE, McKenzie DJ, Wilson RW (2016) A new analysis of hypoxia tolerance in fishes using a database of critical oxygen level (P crit). Conserv Physiol 4:cow012

Sanford LP, Sellner KG, Breitburg DL (1990) Covariability of dissolved oxygen with physical processes in the summertime Chesapeake Bay. J Mar Res 48:567–590

Schmidtko S, Stramma L, Visbeck M (2017) Decline in global oceanic oxygen content during the past five decades. Nature 542:335–339

Shintani T, de la Fuente A, Niño Y, Imberger J (2010) Generalizations of the Wedderburn number: parameterizing upwelling in stratified lakes. Limnol Oceanogr 55: 1377–1389

Vaquer-Sunyer R, Duarte CM (2010) Sulfide exposure accelerates hypoxia driven mortalities. Limnol Oceanogr 55: 1075–1082

Wannamaker CM, Rice JA (2000) Effects of hypoxia on movements and behavior of selected estuarine organisms from the southeastern United States. J Exp Mar Biol Ecol 249:145–163

Wilson BW (1972) Seiches. In: Chow VT (ed) Advances in hydroscience, Vol 8. Academic Press, London

Zhang J, Gilbert D, Gooday AJ, Levin L and others (2010) Natural and human-induced hypoxia and consequences for coastal areas: synthesis and future development. Biogeosciences 7:1443–1467

Editorial responsibility: Just Cebrian, Dauphin Island, Alabama, USA

Submitted: March 12, 2018; Accepted: August 19, 2018
Proofs received from author(s): September 7, 2018